ADVANCED ENERGY MATERIALS
www.advenergymat.de

Scalable Fabrication of Efficient Perovskite Solar Modules on Flexible Glass Substrates

*Xuezeng Dai, Yehao Deng, Charles H. Van Brackle, Shangshang Chen, Peter N. Rudd, Xun Xiao, Yun Lin, Bo Chen, and Jinsong Huang**

Perovskite materials are good candidates for flexible photovoltaic applications due to their strong absorption and low-temperature processing, but efficient flexible perovskite modules have not yet been realized. Here, a record efficiency flexible perovskite solar module is demonstrated by blade coating high-quality perovskite films on flexible Corning Willow Glass using additive engineering. Ammonium chloride (NH_4Cl) is added into the perovskite precursor solution to retard the nucleation which prevents voids formation at the interface of perovskite and glass. The addition of NH_4Cl also suppresses the formation of PbI_2 and reduces the trap density in the perovskite films. The implementation of NH_4Cl enables the fabrication of single junction flexible perovskite solar devices with an efficiency of 19.72% on small-area cells and a record aperture efficiency of 15.86% on modules with an area of 42.9 cm^2. This work provides a simple way to scale up high-efficiency flexible perovskite modules for various applications.

Halide perovskites have attracted great attention as a novel photovoltaic material due to their intriguing optoelectrical properties, solution processability, low cost, and potential for mass production. The power conversion efficiency (PCE) of perovskite solar cells (PSCs) has impressively increased to 25.2%, which is the highest among the next generation solar cells.[1] Due to their large absorption coefficient, the optimal thickness of perovskite films is usually lower than 1 μm, making them an excellent candidate for flexible solar devices. However, the efficiency of flexible PSCs is far behind their rigid counterparts. The highest PCE of flexible PSCs so far is 18.4% from a cell with a small area of 0.052 cm^2.[2] Meanwhile, large-area flexible perovskite solar modules have been rarely reported. The best flexible perovskite solar module has an efficiency of 15.22% with an aperture area of 16.07 cm^2,[3] which is lower than rigid perovskite solar modules.

There are more challenges in developing highly efficient flexible perovskite solar module compared to those made on rigid substrates which come from the commonly used polymer substrates including polyethylene terephthalate (PET) and polyethylene naphthalate (PEN). Indium tin oxide (ITO) is still the best option for the transparent electrode. Deposition of transparent and conductive ITO by sputtering requires a substrate temperature higher than 200 °C to promote crystallization.[4] However, the glass transition temperatures of PET and PEN are around 78 and 120 °C, respectively.[5,6] As a consequence, ITO on polymer substrates has to be deposited at a low temperature such as room temperature, which yields amorphous ITO films. ITO on polymer substrates is much thicker to reduce the sheet resistance, and also less transparent, especially in the wavelength range around 400 nm (Figure S1, Supporting Information).[7,8] In addition, perovskite materials are known to be sensitive to moisture,[9–11] but polymer substrates have relatively high water vapor transmission rates (WVTR). For example, a 100 μm thick PET substrate has a WVTR higher than 3.9 g m^{-2} day^{-1} (at 37.8–40 °C).[12,13] It is not clear yet whether the encapsulation layers for perovskite flexible PV modules made on polymer substrate can still maintain their flexibility or not.

Here, we report fabricating perovskite solar module directly on flexible Willow Glass which itself serves as encapsulation layer. Willow Glass not only retains the advantages of glass substrates, i.e., withstanding processing temperatures over 600 °C and a WVTR below detection limits (3×10^{-7} g m^{-2} day^{-1}),[13] but also offers a good flexibility with the minimum bending radius of less than 100 mm, benefiting from its small thickness, typically 100 μm.[14] The ultrathin glass also enables the manufacturing of lightweight PV modules, fulfilling requirements in emerging markets such as portable power supplies and electric vehicles which need solar panels to be as light as possible. Moreover, the flexible glass is compatible with roll-to-roll fabrication processing, where scalable solution coating strategies such as blade coating and slot-die coating can be applied to realize high throughput and high-speed manufacturing.

We demonstrate a large-area, high-efficiency flexible perovskite solar module with perovskite films fabricated by blade coating on ITO coated Willow Glass. Ammonium chloride (NH_4Cl) was added in precursor solution to improve the perovskite film morphology by retarding perovskite nucleation. Meanwhile, similar to many ammonium halides, NH_4Cl can passivate perovskite films, improving the performance of devices. As a result, the PCE of a flexible perovskite module

X. Dai, Dr. Y. Deng, C. H. Van Brackle, Dr. S. Chen, P. N. Rudd, X. Xiao, Dr. Y. Lin, Dr. B. Chen, Prof. J. Huang
Department of Applied Physical Sciences
University of North Carolina at Chapel Hill
Chapel Hill, NC 27599, USA
E-mail: jhuang@unc.edu

The ORCID identification number(s) for the author(s) of this article can be found under https://doi.org/10.1002/aenm.201903108.

DOI: 10.1002/aenm.201903108

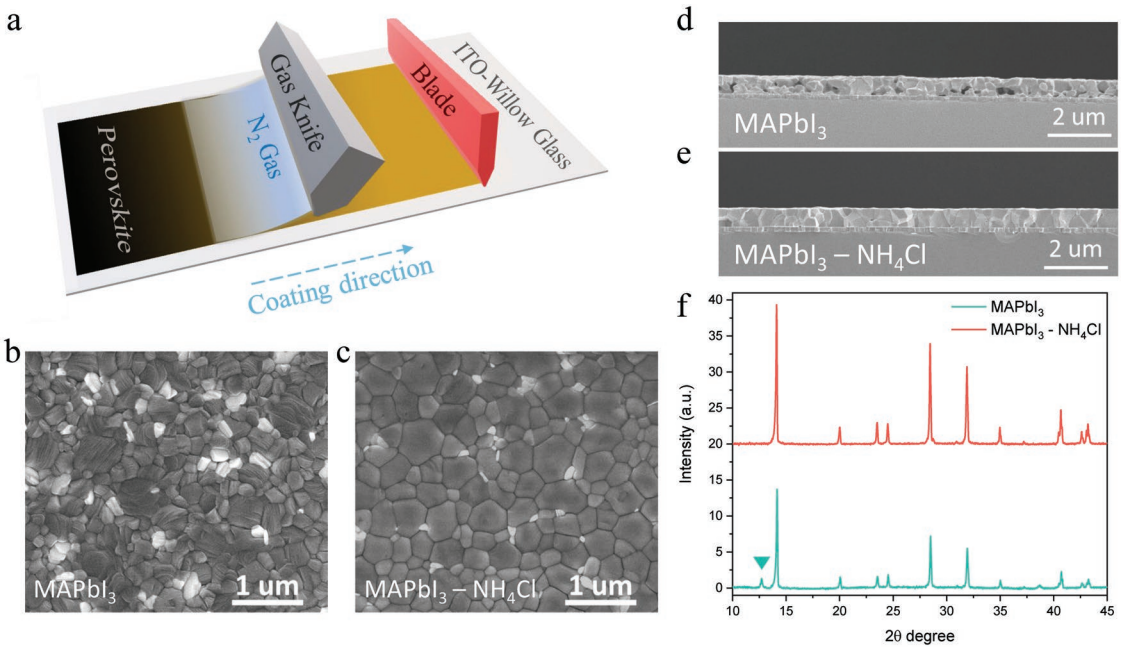

Figure 1. Blade coat perovskite films on ITO-coated Willow Glass with NH_4Cl to improve film morphology and crystallization. a) Schematic illustration of gas-assisted blade coating of perovskite films on ITO–Willow Glass. b,c) Surface SEM images of the blade-coated films without NH_4Cl (b) and with NH_4Cl (c). d,e) Cross-section SEM images of the blade-coated films without NH_4Cl (d) and with NH_4Cl (e). f) XRD patterns of films with and without NH_4Cl.

approaches 16.0% for the first time and is comparable to those made on rigid substrates.

Perovskite films were deposited by gas-assisted blade coating at room temperature in the ambient environment. We intentionally choose room temperature deposition in ambient condition, because this represents realistic manufacturing conditions, which however is much more challenging to do than in glovebox and at elevated temperature. This study leverages a recently developed precursor ink formulation as well as the N_2-knife-assisted fast blading process that enables room-temperature high-speed blading.[15] The coating process is illustrated in **Figure 1**a. The precursor solution of $MAPbI_3$ dissolved in 2-methoxyethanol (2-ME) was injected into the gap between the blade and substrate. The solvent of 2-ME was chosen due to its relatively low boiling point of 124 °C and high vapor pressure of 823 Pa at 20 °C, allowing fast removal of the solvent by gas flowing at room temperature.[16] Moving the blade spreads the film across the substrate; an air knife moving with blade simultaneously blows N_2 gas on the as-coated wet film to remove the solvent, inducing crystallization. In real production, fast processing requires the coating always operates in the Landau–Levich regime where a wet film forms after the blade moves away.[17,18] We tuned the coating speed to the Landau–Levich regime and found that operating between 20 and 100 mm s^{-1} can create continuous and compact perovskite films on the rigid glass substrates, as shown in Figure S2 (Supporting Information).

However, when we followed the same procedure to coat perovskites on Willow Glass, the film coverage is much worse, despite that, the film surface still looks smooth and continuous, containing voids at the interface of perovskites and ITO/glass, as shown in the cross-section scanning electron microscopy (SEM) image in Figure 1d. These void areas reduce the device working area and thus reduce module efficiency. Meanwhile, the perovskite surface shows a relatively large roughness with a root mean square (RMS) of 24.2 nm extracted from the atomic force microscope (AFM), as shown in Figure S3a (Supporting Information). In addition, the X-ray diffraction (XRD) peak at 12.7° (Figure 1f) of perovskite film reveals the presence of PbI_2. The formation of PbI_2 could be induced by the annealing process in the ambient atmosphere, where moisture in air degraded the surface layer of perovskite films. By contrast, when 6×10^{-3} M of NH_4Cl was added into the perovskite precursor solution, the as-coated perovskite films become compact without voids (Figure 1e). The surface gets smoother as well with the RMS roughness reduced to 12.5 nm (Figure S3b, Supporting Information). Moreover, the XRD pattern of films with NH_4Cl (Figure 1f) shows no PbI_2 peaks and the sharper perovskite peaks, indicating better crystallinity. It is well known that films with larger grain size (Figure 1b,c) and better crystallinity are more resistance to moisture,[19] thus reducing the degradation rate during annealing.

To investigate how the NH_4Cl improves the film quality, we monitored the film drying process by a homemade microscopy optical system. The system captured the light transmitted through the films (Transmission mode) or scattered light from the top surface (Reflection mode) with a frame rate of 54 frames s^{-1}. To clearly show the drying process, the solvent was substituted by dimethylformamide, which has a higher boiling point and smaller vapor pressure, to slow down the solvent evaporation. Also, the concentration of NH_4Cl in precursor solution was raised to 0.3 M to amplify the influence. As shown in **Figure 2**a, the wet film without NH_4Cl quickly grew more than 100 μm^{-2} nuclei and turned to dark in 1 s. And, the film remained dark

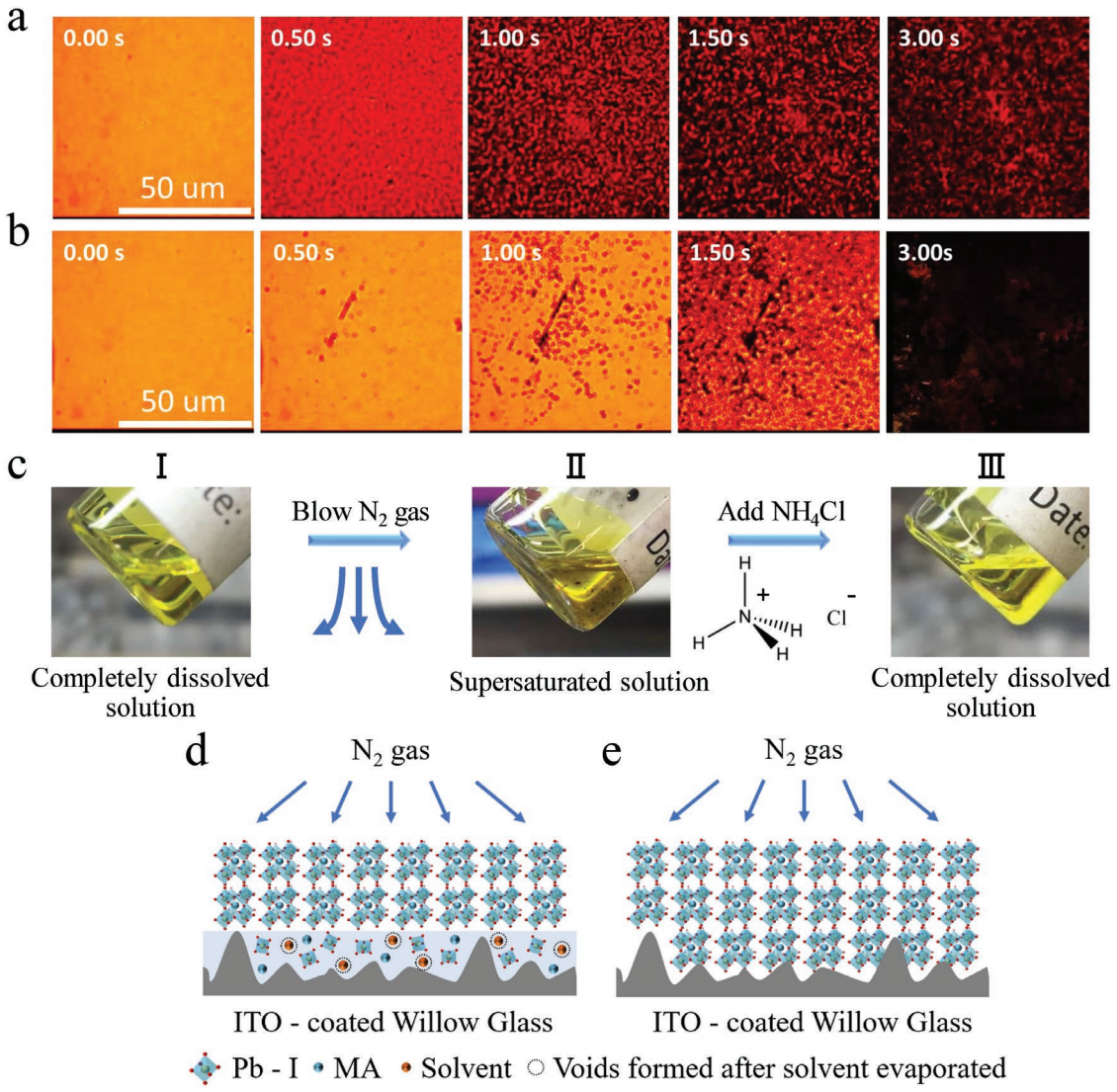

Figure 2. The NH_4Cl improves film morphology by retarding the crystallization rate. a,b) In situ microscopy observation of drying process of the as-coated perovskite film without NH_4Cl (a) and with NH_4Cl (b). c) The enhancement of solubility by the presence of NH_4Cl. d,e) Schematic illustration of the formation of a perovskite capping layer on ITO-coated Willow Glass. The wet film without NH_4Cl forms capping layer fast with trapped solvent in the valleys (d). The NH_4Cl retards the nucleation, enabling nucleation after most solvents evaporated, forming compact film without voids (e).

afterward, indicating the nucleation almost completed in the first second. By contrast, when NH_4Cl was added in the solution, only several microparticles evolved from the whole area in 0.5 s and grew to around 1 μm^{-2} nucleus in 1 s. The nuclei grew slowly and lasted until the film ultimately turned to black in 3 s. The sluggish transformation process suggests suppressed nucleation of intermediate phase by NH_4Cl (Figure 2b). This is attributed to the enhanced solubility of perovskite in the solvent with NH_4Cl. Figure 2c and Figure S4 (Supporting Information) demonstrate direct evidence that NH_4Cl makes the solution more soluble to the perovskite. In Figure 2c, a thoroughly dissolved solution of 2.5 M $MAPbI_3$ in 2-ME (Figure 2c(I)) was blowing under N_2 gas to remove part of the solvent and form a supersaturated solution with black perovskite clusters, as shown in Figure 2c(II). Then, 5 mg mL^{-1} NH_4Cl powder was added in the as-prepared supersaturated solution while stirring under room temperature. The solution quickly turned to clear again, and the clusters were dissolved entirely in 1 min (Figure 2c(IIIs)), indicating the NH_4Cl enhanced the solubility of the solution to dissolve the precipitated perovskite clusters. The solubility enhancement can be attributed to the chemical interactions between NH_4^+ and PbI_2 in precursor solution, in which NH_4^+ is more favorable to form hydrogen bonds with I—Pb—I. This is further confirmed by the ^1H NMR measurement on neat NH_4Cl and NH_4Cl–PbI_2 mixture in methanol-D4 (Figure S5, Supporting Information). The neat NH_4Cl only shows a single sharp peak at 7.42 ppm, which is broadened and shifted to higher field in the NH_4Cl–PbI_2 mixture. The shift of peak can be ascribed to that the hydrogen bonds formed between NH_4^+ and I—Pb—I drag the electrons from N to H and the electron density on proton nucleus becomes higher. In addition, the broadened peak indicates various intermediates

formed between NH_4^+ and PbI_2 via hydrogen bonds that weaken the I—Pb—I bonds and thus increase the solubility of PbI_2 in precursor solution.

The reduced nucleation rate plays a vital role in film formation on the ITO-coated Willow Glass. The AFM results in Figure S6 (Supporting Information) show that the peak–valley height of ITO on Willow Glass reaches up to 70 nm, which is much larger than that (≈15 nm) on rigid glass. The large difference of roughness comes from the existence of the thin buffer layer between the rigid glass and the deposited ITO. It is common to deposit a buffer layer such as SiO_2 underneath ITO to prevent the diffusion of alkali ions in the soda–lime glass from poisoning the ITO. The buffer layer also makes ITO sputtered on it to be smoother.[20,21] On the contrary, Willow Glass is made by alkali-free borosilicate,[14] making the buffer layer unnecessary for transparent conductive substrates. In addition, alkali ions are not shown to be an issue for perovskite solar cells. As a matter of fact, they are frequently shown to benefit the perovskite materials in passivating the defects.[22,23] However, the rough ITO hindered the deposition of dense perovskite films by trapping solvents in the valleys on the ITO surface and slowing down the solvent evaporation. Since the drying gas quickly blew away solvents from the surface of the as-coated wet films, perovskites tended to grow from the top to bottom and formed a capping layer before the remnant solvent at the valley escaped (Figure 2d). The escaping of trapped solvents eventually forms voids, as shown in Figure 1d. Thus, an effective way to prevent the void formation is to remove the solvent before the solid capping layer entirely covers the surface or avoid the solid capping layer formation. Slowed down solidification by NH_4Cl by suppressing nucleation allows most solvent, including that in the valleys, to have sufficient time to escape. We do not see obvious formation of a solid capping layer, since the whole layer dried uniformly. As a result, a dense solid layer formed on ITO without voids (Figures 1e and 2e). Similarly, in Figure 2a, a capping layer quickly formed so that the regions with remnant solvent remaining underneath shows red color at 3 s. On the contrary, a dense film with dark color formed at 3 s by adding NH_4Cl.

The small-area single cells and large-area module were fabricated on flexible substrates. The device structure was MgF_2/Willow Glass/ITO/poly(bis(4-phenyl)(2,4,6-trimethylphenyl) amine (PTAA)/$MAPbI_3$/fullerene (C_{60})/bathocuproine (BCP)/copper (**Figure 3**a). ITO was deposited by magnetron sputtering which has been optimized for flexible Willow Glass. Details about ITO deposition on the Willow Glass can be found in the Experimental Section. A thin layer of MgF_2 (100 nm) was deposited onto glass to reduce reflection of light. The performance of small-area single cells and large-area modules is shown in Figure 3c,d and **Table 1**. The champion cell with NH_4Cl exhibits PCE of 19.72% from reverse scan and 19.29% on forward scan, while that without NH_4Cl only had PCE of 16.57% and 16.14% on reverse and forward scans, respectively. This is the highest reported PCE of flexible perovskite solar cells.[24] Such efficiency is very close to that of 20.10% on rigid substrate by the same fabrication process (Figure S7, Supporting Information). The comparable efficiencies attribute to the similar transparency and conductivity of the ITO electrodes, as well as the high-quality compact perovskite films on both the substrates. The device with NH_4Cl also has higher external quantum efficiency (EQE) at most wavelengths (Figure S8, Supporting Information) which may be due to better perovskite–hole transport layer contact which facilitates carrier transport. A fabricated large-area module is shown in Figure 3b made by scalable blade coating, where 12 subcells are connected in series. The geometric fill factor (FF) is 92%, as illustrated in Figure S9 (Supporting Information). A champion module with an aperture area (i.e., including dead area) of 42.9 cm^2 achieved PCE of 15.86% under reverse scan with little hysteresis. The efficiency distribution of 15 flexible modules is shown in Figure S10 (Supporting Information), giving an average PCE of 14.34%. As shown in Figure 3e, the photocurrent of the champion module stabilized within seconds, yielding a stabilized PCE of 15.62%. The average V_{OC} of each subcell is 1.095 V, the same as a single cell, indicating good uniformity of the films over a large area. The J_{SC} of 19.71 mA cm^{-2} was calculated from the aperture area of each subcell. The reduced FF of 73.5% compared to small cells (79.1%) can be ascribed to the larger series resistance due to the longer paths that the carriers transport through the ITO and copper electrodes or the nonuniformity of the devices. Figure 3f summarizes the performance of recently reported flexible perovskite modules versus their device area, showing this is the largest and most efficient flexible perovskite module reported so far.

To unveil the additional functions of the NH_4Cl, further characterization was performed. First, the leakage current density of the flexible cells reduced by over an order of magnitude by adding NH_4Cl (**Figure 4**a), which is mainly due to the formation of dense perovskite films without voids. The smaller dark current density agrees with the improvement of the fill factor of the flexible cells (Figure 3c and Table 1). To study the charge carrier recombination dynamics, time-resolved photoluminescence (TRPL) was measured. The photoluminescence (PL) transient curves for the films with and without NH_4Cl showed a biexponential decay. The additive molecule reduces the decay of the fast process and increases the slow process from 130 to 217 ns (Figure 4b), which can be attributed to reduced nonradiative recombination losses in the $MAPbI_3$–NH_4Cl film. Moreover, steady-state PL measurements (Figure 4c) showed a notable enhancement of the PL intensity in the film using the NH_4Cl additive, as well as a small blueshifted peak position, indicating less trap states. The trap density of states (tDOS, Figure 4d) measured by thermal admittance spectroscopy (TAS) gives the same conclusion. The previous works established that the shallower traps states (below 0.50 eV) are attributed to those traps along grain boundaries, while the deeper traps states (above 0.50 eV) correspond to surface traps.[26,27] The reduction of shallower trap density is mainly attributed to the enlargement of the grain size by NH_4Cl (Figure 1c), which reduced the total area of grain boundaries. NH_4Cl treatment did not have obvious impact on very deep traps, indicating that the surfaces were not strongly impacted.

In summary, we demonstrate for the first time a large-area flexible perovskite module on Corning Willow Glass with efficiency approaching 16%. The features of Willow Glass enable the manufacture of a high transparency, low sheet resistance, flexible conductive substrate. The large-area, high-quality perovskite films were realized by a scalable blade coating strategy. NH_4Cl additive was shown to effectively form compact

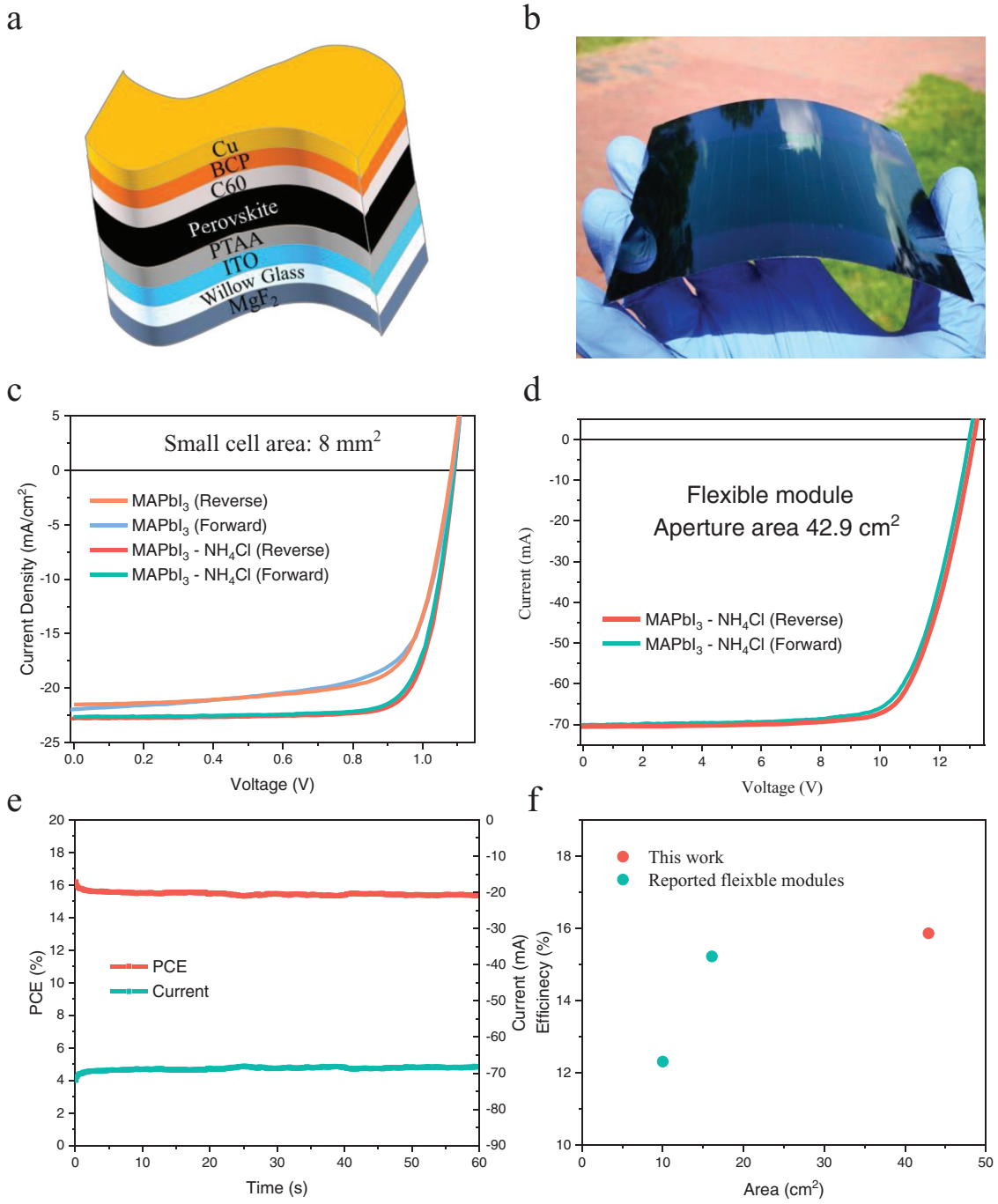

Figure 3. Performance of flexible perovskite small-area cells and large-area modules. a) Schematic illustration of the flexible perovskite device structure. b) Photograph of a flexible perovskite module. c) *J–V* curve of small-area flexible perovskite cells with and without NH_4Cl in the precursor solution. d) *I–V* curve of the champion flexible perovskite modules with NH_4Cl in the precursor solution. e) Steady-state measurement of the current and PCE of the champion flexible perovskite solar module. f) Power conversion efficiencies of flexible perovskite modules as a function of module area from this work and other reports.[3,25]

perovskite films and passivate defects. The blade coating and flexible Willow Glass used here are fully compatible with the high throughput roll-to-roll process. Also, Willow Glass acts as a moisture barrier, saving an encapsulation procedure and lowering the production cost. Taken together, our results provide a new opportunity for the mass production of the low-cost, lightweight, and high-efficiency flexible perovskite solar panels.

Experimental Section

Materials: Unless stated otherwise, all materials and solvents were purchased from Sigma-Aldrich. MAI was purchased from GreatCell Solar. All chemicals were used as received without further purification. Methylammonium hypophosphite was synthesized according to our previous publication.[28] Corning Willow Glass (thickness: 100 µm) substrates were received from Corning Research & Development Corporation.

Table 1. Photovoltaic parameters of the flexible perovskite small-area cells and large-area modules.

	V_{OC} [V]	J_{SC} [mA cm^{-2}]	FF [%]	η [%]
$MAPbI_3$ (Reverse)	1.083	21.49	71.2	16.57
$MAPbI_3$ (Forward)	1.086	21.95	67.7	16.14
$MAPbI_3$–NH_4Cl (Reverse)	1.092	22.83	79.1	19.72
$MAPbI_3$–NH_4Cl (Forward)	1.090	22.66	78.1	19.29
Flexible module (Reverse)	13.142	19.71	73.5	15.86
Flexible module (Forward)	12.995	19.61	72.8	15.45

Transparent Conductive Flexible Substrate Fabrication: The Willow Glass substrates were cleaned by ultrasonication with deionized (DI) water, acetone, and isopropanol sequentially. The ITO was sputtered in a Lesker Sputter system (PRO Line PVD 75) with low power of 100 W (radio frequency (RF) mode) under a 3 mTorr mixed gas of Ar and O_2. The substrate was heated to 270 °C during sputtering to increase the crystallinity of ITO film. The thickness of ITO layer was 130 nm.

The ITO was etched in a cleanroom to make patterns for small devices and modules. The ITO/Willow Glass was first spin-coated with an adhesive primer (MCC Primer 80/20, MicroChem) and positive photoresist (MICROPOSIT S1813, MicroChem) at 3000 rpm for 40 s sequentially. The coated substrates were soft baked at 115 °C on a hot plate for 1 min. After UV exposure 10 s through a photomask, the substrate was immersed and wobbled in a photoresist developer (MICROPOSIT, MF-319, MicroChem) for 1 min. Then, it was washed by DI water and dried by N_2 gas gun. The substrate with patterned photoresist was immersed in acid solution (H_2O:HCl:HNO_3 = 50:50:3) for 5 min to etch the ITO area not covered by photoresist. The etching solution was heated to 65 °C to accelerate the etching rate. The etched substrate was washed by Na_2CO_3 solution (0.1 g L^{-1}) and DI water. The dried substrate was exposed to UV light for another 10 s without photomask, then removed the whole photoresist layer by immersing in developer again. Then, it was washed and dried to finish the patterned process.

Device Fabrication: The fabrication was conducted under temperature between 20 and 22 °C and with a relative humidity between 30% and 50%. The patterned flexible ITO substrate was cleaned by ultrasonication with deionized water, acetone, and isopropanol sequentially. The dried substrate was then subjected to UV-ozone treatment for 15 min. 3.3 mg mL^{-1} PTAA dissolved in toluene was blade-coated on the substrate at 20 mm s^{-1} with a 150 µm coating gap. The holes on the blade stage were keeping a vacuum to hold the flexible substrate during coating. Then, the perovskite layer was blade-coated under air knife blowing in the ambient environment. Specifically, L-α-phosphatidylcholine and methylammonium hypophosphite were added into ≈1.45 M $MAPbI_3$/2-ME solution in a concentration of ≈0.3 mg mL^{-1} and ≈0.15 vol%, respectively. For optimized films, 6×10^{-3} M NH_4Cl was added in the precursor solution. The gap between blade and substrate was 250 µm. The flowing gas pressure was 20.0 psi. The blade and air knife moving speed was 20 mm s^{-1}. The as-coated film was transferred to hot plate annealing at 95 °C for 10 min. The film then was thermally evaporated with 30 nm C_{60} and 6 nm BCP. For the flexible module, P2 was cut using laser scribing strategy. Then, the scribed film was evaporated with 150 nm copper electrode. The flexible module was scribed P3 to complete the series connection. The devices were evaporated 100 nm MgF_2 on the back of the flexible Willow Glass before test.

Characterizations: The in situ optical images of film drying were captured by a home-made optical system which included a fast

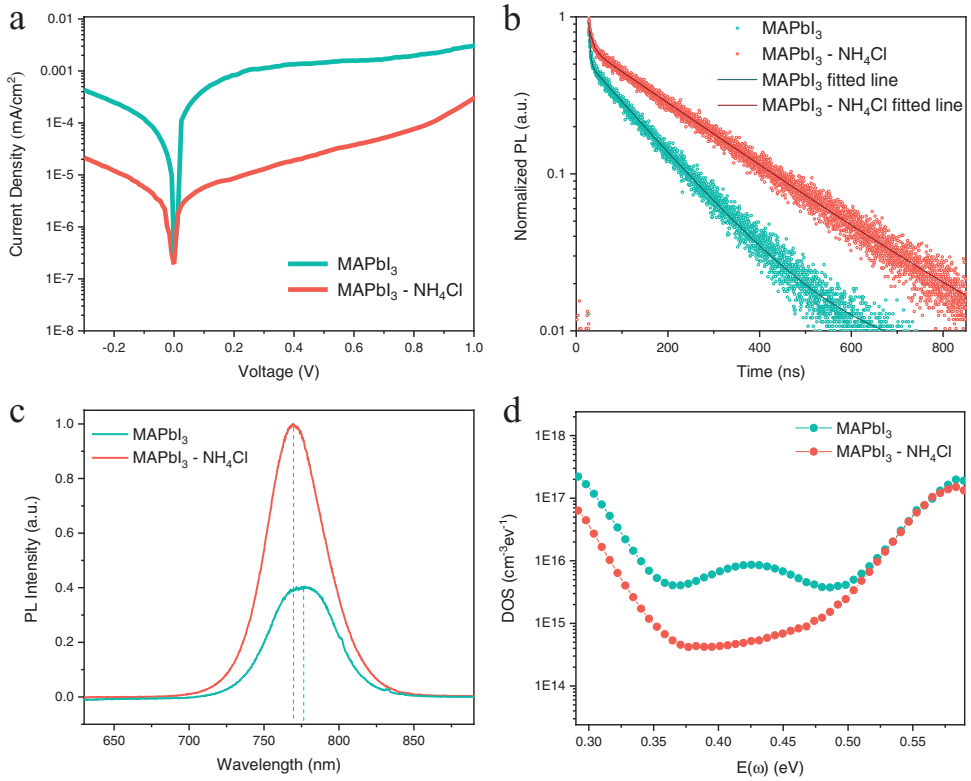

Figure 4. Characterizations of the films and devices. a) Dark current densities of small-area flexible perovskite devices with and without NH_4Cl. b,c) TRPL transients (b) and PL (c) spectra of perovskite films with and without NH_4Cl. d) Trap density of states (tDOS) obtained from thermal admittance spectroscopy (TAS) measurement of small-area flexible perovskite devices with or without NH_4Cl.

microscope camera with a frame rate of 54 frames s^{-1}. SEM images were taken on FEI Helios 600 Nanolab Dual Beam System. The AFM images were scanned from an Asylum Research MFP3D Atomic Force Microscope. The current–voltage measurements were recorded with a Keithley 2400 Source-Meter under simulated AM 1.5G irradiation produced by a Xenon lamp–based solar simulator (Oriel Sol3A, Class AAA Solar Simulator). The light intensity was calibrated using a silicon reference cell with a KG5 glass filter (Newport 91150 V). The scan rate was 0.1 V s^{-1}. The dark current density of devices was recorded on the same Keithley 2400 Source Meter in dark room. The devices were covered with a black box. EQE was obtained by a Newport QE measurement kit which focused a monochromatic beam onto the working area of the device. The XRD patterns were performed on a Rigaku MiniFlex X-ray diffractometer. Steady-state PL spectra were measured with a Horiba iHR320 imaging spectrometer. A 532 nm green laser (Laserglow Technologies) with an intensity of 100 mW cm^{-2} was used as the excitation source. TRPL was obtained using a DeltaPro time-correlated single photon counting (TCSPC) filter fluorometer with a pulsed laser source at 406 nm (Horiba NanoLED 402-LH; pulse width below 200 ps, 20 pJ per pulse, ≈1 mm2 spot size), and the signal was recorded using TCSPC. The ^{1}H NMR spectra were recorded on a Bruker NEO 400 MHZ NMR spectrometer. Chemical shifts were reported in parts per million (ppm, δ). ^{1}H NMR spectra were referenced to tetramethylsilane (0 ppm) for methanol-D4.

Supporting Information

Supporting Information is available from the Wiley Online Library or from the author.

Acknowledgements

This work was supported by the Office of Naval Research under Award No. N00014-17-1-2619, the UNC Research Opportunities Initiative (ROI) through the Center of Hybrid Materials Enabled Electronic Technology. This work was performed in part at the Chapel Hill Analytical and Nanofabrication Laboratory, CHANL, a member of the North Carolina Research Triangle Nanotechnology Network, RTNN, which was supported by the National Science Foundation, Grant No. ECCS-1542015, as part of the National Nanotechnology Coordinated Infrastructure, NNCI.

Conflict of Interest

The authors declare no conflict of interest.

Keywords

blade coating, flexible, high efficiency, modules, perovskites

Received: September 21, 2019
Revised: October 27, 2019
Published online: November 21, 2019

[1] NREL PV Research Cell Record Efficiency Chart, https://www.nrel.gov/pv/cell-efficiency.html (accessed: October 2019).
[2] J. Feng, X. Zhu, Z. Yang, X. Zhang, J. Niu, Z. Wang, S. Zuo, S. Priya, S. F. Liu, D. Yang, *Adv. Mater.* **2018**, *30*, 1801418.
[3] T. Bu, J. Li, F. Zheng, W. Chen, X. Wen, Z. Ku, Y. Peng, J. Zhong, Y.-B. Cheng, F. Huang, *Nat. Commun.* **2018**, *9*, 4609.
[4] P. Lippens, U. Muehlfeld, *Handbook of Visual Display Technology*, Springer, Cham, Switzerland **2016**.
[5] W. A. MacDonald, M. Looney, D. MacKerron, R. Eveson, R. Adam, K. Hashimoto, K. Rakos, *J. Soc. Inf. Disp.* **2007**, *15*, 1075.
[6] K. Ngai, S. Capaccioli, *Phys. Rev. E* **2004**, *69*, 031501.
[7] V. Zardetto, T. M. Brown, A. Reale, A. Di Carlo, *J. Polym. Sci., Part B: Polym. Phys.* **2011**, *49*, 638.
[8] C. Wang, L. Guan, D. Zhao, Y. Yu, C. R. Grice, Z. Song, R. A. Awni, J. Chen, J. Wang, X. Zhao, *ACS Energy Lett.* **2017**, *2*, 2118.
[9] J. A. Christians, P. Schulz, J. S. Tinkham, T. H. Schloemer, S. P. Harvey, B. J. T. de Villers, A. Sellinger, J. J. Berry, J. M. Luther, *Nat. Energy* **2018**, *3*, 68.
[10] W. Q. Wu, Z. Yang, P. N. Rudd, Y. Shao, X. Dai, H. Wei, J. Zhao, Y. Fang, Q. Wang, Y. Liu, Y. Deng, X. Xiao, Y. Feng, J. Huang, *Sci. Adv.* **2019**, *5*, eaav8925.
[11] Y. Bai, Y. Lin, L. Ren, X. Shi, E. Strounina, Y. Deng, Q. Wang, Y. Fang, X. Zheng, Y. Lin, Z. Chen, Y. Du, L. Wang, J. Huang, *ACS Energy Lett.* **2019**, *4*, 1231.
[12] Q.-H. Lu, F. Zheng, in *Advanced Polyimide Materials* (Ed: S.-Y. Yang), Elsevier, Amsterdam, Netherlands **2018**, p. 195.
[13] S. M. Garner, S. C. Lewis, D. Q. Chowdhury, presented at *2017 24th Int. Workshop on Active-Matrix Flatpanel Displays and Devices (AM-FPD)*, Kyoto, Japan, July **2017**.
[14] M. Junghähnel, S. Garner, *Vak. Forsch. Prax.* **2014**, *26*, 35.
[15] Y. Deng, X. Dai, C. H. Van Brackle, J. Zhao, B. Chen, J. Huang, *Sci. Adv.* **2019**, *5*, eaax7537.
[16] K. H. Hendriks, J. J. van Franeker, B. J. Bruijnaers, J. A. Anta, M. M. Wienk, R. A. Janssen, *J. Mater. Chem. A* **2017**, *5*, 2346.
[17] Y. Deng, X. Zheng, Y. Bai, Q. Wang, J. Zhao, J. Huang, *Nat. Energy* **2018**, *3*, 560.
[18] X. Dai, Y. Deng, C. H. Van Brackle, J. Huang, *Int. J. Extreme Manuf.* **2019**, *1*, 022004.
[19] Q. Wang, B. Chen, Y. Liu, Y. Deng, Y. Bai, Q. Dong, J. Huang, *Energy Environ. Sci.* **2017**, *10*, 516.
[20] J.-M. Lee, B.-H. Choi, M.-J. Ji, Y.-T. An, J.-H. Park, J.-H. Kwon, B.-K. Ju, *Thin Solid Films* **2009**, *517*, 4074.
[21] X. Ding, J. Yan, T. Li, L. Zhang, *Vacuum* **2011**, *86*, 443.
[22] C. Bi, X. Zheng, B. Chen, H. Wei, J. Huang, *ACS Energy Lett.* **2017**, *2*, 1400.
[23] M. Abdi-Jalebi, Z. Andaji-Garmaroudi, S. Cacovich, C. Stavrakas, B. Philippe, J. M. Richter, M. Alsari, E. P. Booker, E. M. Hutter, A. J. Pearson, S. Lilliu, T. J. Savenije, H. Rensmo, G. Divitini, C. Ducati, R. H. Friend, S. D. Stranks, *Nature* **2018**, *555*, 497.
[24] D. Yang, R. Yang, S. Priya, S. Liu, *Angew. Chem., Int. Ed.* **2019**. *58*, 4466.
[25] T. Bu, S. Shi, J. Li, Y. Liu, J. Shi, L. Chen, X. Liu, J. Qiu, Z. Ku, Y. Peng, *ACS Appl. Mater. Interfaces* **2018**, *10*, 14922.
[26] Y. Shao, Z. Xiao, C. Bi, Y. Yuan, J. Huang, *Nat. Commun.* **2014**, *5*, 5784.
[27] Q. Wang, Y. Shao, Q. Dong, Z. Xiao, Y. Yuan, J. Huang, *Energy Environ. Sci.* **2014**, *7*, 2359.
[28] Z. Xiao, D. Wang, Q. Dong, Q. Wang, W. Wei, J. Dai, X. Zeng, J. Huang, *Energy Environ. Sci.* **2016**, *9*, 867.